HHS Public Access

Author manuscript

Neuron. Author manuscript; available in PMC 2017 December 21.

Published in final edited form as:

Neuron. 2016 December 21; 92(6): 1213–1219. doi:10.1016/j.neuron.2016.11.008.

Linking Electrical Stimulation of Human Primary Visual Cortex, Size of Affected Cortical Area, Neuronal Population Activity, and Subjective Experience

Jonathan Winawer[1] and **Josef Parvizi**[2]

[1]New York University, New York, USA

[2]Stanford University, Stanford, California, USA

Summary

Electrical brain stimulation (EBS) complements neural measurements by probing the causal relationship between brain and perception, cognition, and action. Many fundamental questions about EBS remain unanswered, including the spatial extent of cortex responsive to stimulation, and the relationship between the circuitry engaged by EBS and the types of neural responses elicited by sensory stimulation. Here, we measured neural responses and the effects of EBS in primary visual cortex in four patients implanted with intracranial electrodes. Using stimulation, behavior, and retinotopic mapping, we show the relationship between the size of affected cortical area and the magnitude of electrical charge. Furthermore, we show that the spatial location of electrically induced visual sensations is matched to the receptive field of the cortical site measured with broadband field potentials, and less so with event related potentials. Together, these findings broaden our knowledge about the mechanism of EBS and the neuromodulation of the human brain.

eTOC blurb

We quantified the area of cortical tissue activated by electrical brain stimulation in human patients. The location of phosphenes evoked by stimulating primary visual cortex matched the receptive field of the cortical site measured with broadband field potentials.

Introduction

Focal stimulation of human cerebral cortex has long been known to elicit (Bartholow, 1874; Brindley and Lewin, 1968; Dobelle and Mladejovsky, 1974; Penfield and Perot, 1963), or interfere with (Ojemann et al., 1989), specific and complex behaviors and experiences, making it a powerful tool for investigating the cortical basis for perception, thought and behavior. EBS studies in nonhuman primates have greatly advanced our understanding of

Author Contributions

JW and JP designed and executed the studies. JP conducted EBS experiments. JW analyzed data. JW and JP wrote the manuscript.

sensory processing and perceptual decision-making (Cohen and Newsome, 2004; Salzman et al., 1990), and studies in other mammalian brains have begun to uncover the fine-grained effects of EBS (Histed et al., 2009).

While past studies in animals have yielded important knowledge about microstimulation of the brain (Tehovnik and Slocum, 2007), much remains to be known about the effect of EBS in the human brain. Typical animal and human EBS studies differ 1,000 fold in electrode diameter, impedance, and electrical current. Thus, the generalizability from animal models to clinical neuromodulation is unknown (Borchers et al., 2012).

To study the effect of EBS on human cerebral cortex, we took advantage of the topographic organization of primary visual cortex (V1) to (1) quantify the size of affected cortical area as a function of electrical charge using a novel, model-based approach, and (2) assess how the circuitry engaged by EBS relates to neural signals elicited by sensory stimulation.

Four patients with focal epilepsy were implanted with intracranial electrodes for intracranial EEG monitoring (Table S1). EBS was applied to pre-selected V1 electrodes (Figure 1a, b), outside the patients' pathological zones, using square-wave pulses with varying frequency (5–100Hz), pulse width (200–1,000μs), amplitude (0.2–5mA) and duration (0.2–1s) (Table S2). EBS produced localized visual sensations (phosphenes) (Foerster, 1929), quantified in two ways: subjects outlined the phosphene on a computer screen following stimulation (sites 1–5), and rated the intensity of the phosphene on a 0–10 scale (sites 2, 3, and 5). There were 0 false positives and only 4 false negatives (13 shams stimulations, 102 trials; Table S2). In a control experiment, we confirmed the reliability of each subject's tracing (Figure S2).

RESULTS

Separating ECoG signals into component responses

In each subject, we recorded intracranial electrophysiological signals (ECoG) from the stimulated site. The local field potential measured by ECoG shows a response when the stimulus is in the site's population receptive field ('pRF' (Dumoulin and Wandell, 2008; Yoshor et al., 2007)). Since the ECoG signal sums the responses generated by multiple types of neural sources (Buzsaki et al., 2012), we separated the visually driven ECoG response into two complementary components: the steady state visual evoked potential, which is time-locked to the visual stimulus (Adrian and Matthews, 1934; Norcia et al., 2015), and broadband power, which is a rise in the variance in response to a stimulus (Miller et al., 2014) (Figure 1c, d). This rise in variance is superimposed on a power spectrum approximately of the form, $power \propto \frac{1}{f^n}$, where f is the temporal frequency and n is a constant (Miller et al., 2009; Milstein et al., 2009). This constant n in our data, computed for the blank stimulus conditions over the range 10–200Hz was approximately 2.6 (2.9. 2.2, 2.9, 2.4, 2.6; sites 1–5). Prior work has shown that broadband and evoked potentials pool spatial information differently and likely arise from different neuronal population and network activity (Winawer et al., 2013). The broadband signal clearly spans a wide frequency range (10 to 200Hz; Figure 1c), although in other studies this signal is most evident in the high frequencies, and hence is often referred to as "high gamma" or "high frequency broadband" (Canolty et al., 2006; Crone et al., 1998).

Overlap between Phosphenes and ECoG pRFs

The overlap between EBS phosphenes and ECoG pRFs was best for the ECoG broadband response. For each site, separate pRFs were computed from the broadband and stimulus-locked time series (Figure 2a, b). The two types of pRFs yielded similar but not identical solutions (Figure 2c). They did not differ substantially in accuracy, with an average variance explained for the five sites of 80.8% for the broadband pRF and 80.5% for the stimulus-locked pRF (Figure 2d, inset, and columns 2&3 in Table S3), indicating that models from each component of the ECoG signal provided excellent fits to the corresponding time series.

For sites 1–4, the phosphenes were better matched to the pRFs derived from the broadband time series than the stimulus-locked time series (Figure 2c). For site 5, corresponding to the fovea (<1°), the pRFs were much larger than the phosphenes, likely due to challenges of accurately measuring very small receptive fields near the central fovea (Dougherty et al., 2003). These observations were quantified by computing a measure of overlap, the Dice coefficient, between either the broadband or stimulus-locked pRF for a given site (thresholded to within 2 standard deviations of the Gaussian pRF) and each of the phosphenes drawn by the subjects when that site was stimulated (Figure 2d, Figure S3). For sites 1–4, the overlap coefficient was significantly higher for the broadband pRFs than the stimulus-locked pRFs (p=0.020, 0.000, 0.000, 0.006; tests of bootstrapped means, Table S3). For site 5, the overlap coefficient was significantly higher for the stimulus-locked pRF (p=0.000), though the overlap coefficient was low for both measures (less than 0.03, 5–20 times less than the coefficients for the other 4 channels).

Effect of Stimulation Parameters on Size of Phosphenes and Responsive Cortex

Across EBS trials, the phosphenes on average showed a high level of overlap with broadband pRFs measured from the same electrode. The phosphenes, however, were not identical on each trial, and tended to be larger on trials with greater electrical charge (Table S2). We took advantage of these trial-to-trial differences to quantify the spatial extent of activated cortex as a function of electrical charge. To do so, we devised a model that relied on the retinotopic map of V1, derived from preoperative fMRI or by fitting a template to the subject's anatomical MRI (Benson et al., 2014). From the retinotopic map, we know the relationship between locations in the visual field and locations on cortex. The spatial overlap between fMRI, broadband ECoG, and EBS phosphenes (Figure 3a–c) indicates that it is reasonable to assume that the V1 response near the electrode corresponds to the spatial location of the phosphenes. To quantify the relationship between electrical charge and the size of the cortical area affected by EBS, we projected the subjects' phosphene outlines onto the same subject's V1 map, yielding a measure of cortical area for each EBS trial (Figure 3d). We then asked how the phosphene area in the visual field and the phosphene area projected onto cortex varied with electrical charge.

The relationship between charge and phosphene size in the visual field showed two clear patterns: Stimulating with more charge or stimulating more peripheral receptive fields caused larger phosphenes (Figure 4a). The cortical area of phosphenes also increased as a function of charge deposited (Figure 4b), but did not differ systematically as a function of eccentricity. The apparent discrepancy between phosphene size in the visual field and on

cortex is reconciled by the pattern of cortical magnification in V1. In the portion of V1 representing the peripheral visual field, a small amount of tissue responds to a large region in the visual field, whereas in the part of V1 that represents the central visual field, the same amount of tissue responds to only a very small part of the visual field (Figure 4c). Therefore, even though for a given amount of charge the phosphene areas in the visual field spanned a range of about 1000:1 across sites, the area of activated cortex was tightly clustered. Notably, as the charge increased, the area of activated cortex spread well beyond the size of the electrode (Figure 4b, data points above the dotted lines). The implication is that electrical stimulation cannot be assumed to interact with only cortical regions directly below the stimulated electrode. Rather, with stimulation parameters within the range used for standard clinical testing, we estimate the spatial spread to include an area up to $1cm^2$. The functions fit to phosphene size were power laws, with the exponents less than 1 (Table S4, column 2), indicating that the effect of increasing electrical charge declined with higher stimulation levels, suggesting that the spatial spread saturates with high charge.

Effect of Stimulation Parameters on Subjective Ratings

In addition to obtaining phosphene outlines, for 3 sites we also asked subjects to provide a numerical rating of the intensity of the phosphene. Some of the subjects also offered additional, spontaneous descriptions of phosphene properties (e.g., color, motion), but only the size, location, and intensity of their perceptual change were consistently recorded and thus quantifiable.

Like cortical surface area, subjective ratings increased with charge deposited at each site tested but did not depend systematically on the eccentricity of the pRF (Figure 4d). The ratings were most reliable for very low or very high charge, with ratings of 1 or 2 for all trials with charge below 10μC, and 9 or 10 for all trials with charge above 100μC. For intermediate charge – between 10 and 100μC – ratings ranged from 1 to 9. This pattern suggests that perceived intensity, like phosphene size, increased rapidly over intermediate charges and slowly at higher charges. The power law exponent fitted to the ratings ranged from 0.17 and 0.44 (Table S4), indicating that the effect of increasing stimulation decreased at higher stimulation levels.

Next, we separated the charge deposited per site into two complementary components, the amount of charge per phase and the frequency of stimulation. Both parameters influenced the size of the phosphene projected to the cortex: If either the frequency was low (below ~15Hz) or the charge per phase was low (below ~0.7μC), the area of responsive tissue on the cortex area was small (Figure 4e, left). In contrast, the subjective rating of intensity only depended systematically on the frequency of stimulation, and not on the charge per phase (Figure 4e, right). The difference in these patterns illustrates the value of obtaining multiple quantitative behavioral measures. (See Figure S4 for multiple regression fits.)

DISCUSSION

Our findings are based on a model-based approach to integrate EBS with retinotopic maps, and as such they provide, to our knowledge, the first quantification of the spatial extent of brain tissue affected by EBS in human cerebral cortex. Our results complement estimates

made in macaque V1 for stimulation with microelectrodes, using very different stimulation parameters (Tehovnik and Slocum, 2007). Further, the results demonstrate a close quantitative match between visual perception evoked by EBS and neurophysiological responses measured from the human brain. This fact does not bear on the question of whether V1 activity, on its own, is critical for visual awareness (Crick and Koch, 1995), as EBS-induced electrical discharges in V1 propagate to other areas of the brain, enabling the subject to make overt judgments about their experience.

In our data, the broadband ECoG response was the neurophysiological measure that best matched subjective experience, as indexed by the overlap between pRFs and phosphene. These results raise the question of why the pRFs measured by two components of the ECoG time series differ. We consider several possible answers.

First, it might be the case that the two types of pRFs are in fact similar, but that the ERPs have lower signal to noise ratio, leading to a poorer estimation of the pRF for the stimulus locked signal. This explanation is unlikely, since the evoked signal is large and the variance explained by the two pRF models was nearly identical. Second, the sizes of the neural receptive fields giving rise to the two types of pRFs might differ. This is plausible as different cell types and lamina within the same cortical site can vary substantially in the spatial extent of their responses., as suggested by the large spread of activity in superficial layers measured with voltage sensitive dye (Palmer et al., 2012). However, this explanation would lead to differences in pRF *size*, whereas we also observe differences in pRF *location*. Hence this is unlikely to be the complete explanation. A third possibility arises from the fact that the spatial sensitivity of the LFP is highly dependent on the structure of the neural activity, with coherent signals having a significantly longer reach than incoherent signals (Linden et al., 2011). The implication is that the broadband signal, assuming it has incoherent sources, is dominated by sources close to the electrode (Liu and Newsome, 2006), and is therefore likely a good match to the neurons influenced by EBS. In contrast, the stimulus-locked potential is likely influenced by neurons located at a greater distance. The effect of distance on the pRF will depend on an interaction of the local cortical geometry and the retinotopic map. Finally, we note that cortical generators of the evoked potential (stimulus-locked signal) are not yet fully understood. In cat V1, the evoked potential carries non-retinotopic stimulus information as well as retinotopic (Kitano et al., 1994; Mitzdorf, 1987), which may influence estimates of the receptive field. The broadband signal has been shown to be correlated with both the local BOLD signal and multiunit spiking activity, and likely better reflects the neural activity directly beneath the electrode (Winawer et al., 2013 and references within).

We quantified the effect of EBS on subjective experience with phosphene outlines and numerical ratings. As with all subjective measures, it is important to consider the accuracy with which subjects report their experience. We used an outline task to measure perception with reference to the spatial coordinates of the outline in the tradition of input-referred measures in sensory neuroscience (Wandell, 1995). The outlines on control trials were accurate (matching the visual stimulus) and reliable across repeated trials, providing confidence in the reliability of subjects outlining the phosphene areas. The method was also validated by the high degree of overlap between the EBS outlines and the pRFs from the

corresponding electrodes, which do not depend on subjective reports. Rating the intensity of the phosphenes is a less well-defined task and is not measured in physical units. This type of task is in the psychophysical tradition of magnitude estimation (Stevens, 1957). The dependency of ratings on EBS parameters was not identical to the dependency of phosphene area on the EBS parameters, suggesting that the two metrics provide complementary information. As in previous studies of magnitude estimation, the ratings approximately followed a power law. This, and the lack of false positives in sham trials, indicate a degree of validation for this metric.

While our findings have practical implications for the field of neuromodulation, and help us understand better the human EBS literature, several questions remain to be answered: For instance, is the charge spread independent of the cytoarchitecture of the cortical tissue being stimulated; how does the duration of the phosphene depend on the duration of stimulation; and how do the spatial extent and selectivity of the circuits engaged by intracranial EBS compare to stimulation with extracranial techniques used for clinical treatments? These and many more questions were beyond the scopes of the present study and will be explored in future studies.

Experimental Procedures

Participants

Four adult patients with focal epilepsy were implanted with intracranial electrodes unilaterally for clinical reasons to localize the source of seizures (age 24 to 40; Table S1). Patients signed informed consent for participation in our study, which was approved by the Stanford University Institutional Review Board.

Electrode localization

Electrodes were implanted as either strips or grids (AdTech Medical Instrument Corp, Racine, Wisconsin, USA). Five electrodes were used for analysis from the four patients, all recording from V1 (Table S3). Each electrode was a platinum plate, either 2.3mm or 1.15mm in diameter (exposed recording area) with center-to-center spacing of 4–10 mm between adjacent electrodes on the grid or strip. The electrode positions were identified on post-operative computed tomography (CT) images. The CT images were aligned with the preoperative anatomical MRIs using a method described by Hermes et al (2010).

Anatomical and Functional MRI

MRI sessions were conducted to localize visual field maps and electrode positions. The MRI session took place prior to electrode implantation. In two subjects, we acquired both functional and anatomical MRI (S1 and S3). For S2 and S4, we acquired only anatomical MRI, and derived retinotopic maps from the subject’s individual anatomy using a retinotopic template (Benson et al., 2014). To verify that each of the electrodes under study was located in V1, two methods were used. First, a V1-V3 template was applied to the T1-weighted whole brain anatomy, and second, a V1 probabilistic atlas was derived from the same T1-weighted anatomy using Freesurfer (Figure 1a, b).

Electrophysiological Recording and Artifact Rejection

We recorded signals with a 128-channel recording system made by Tucker Davis Technologies (http://www.tdt.com/). Off-line, data were re-referenced to the common average, excluding channels with large artifacts or epileptic activity, as determined by the patient's neurologist (author JP).

Visual Mapping Stimuli

Methods for ECoG and fMRI visual field mapping experiments were reported previously in detail (Winawer et al., 2013). A summary of the methods as well as differences from the previous work are described in the Supplemental Methods.

PRF model fitting

The pRF models were computed as described previously, using a 'Compressive Spatial Summation' variant of the linear pRF model (Kay et al., 2013) for the broadband time series and a linear model for the stimulus locked time series (Eq S1). Formulae and fitting procedures are described in the Supplemental Methods.

Broadband and Stimulus-locked ECoG Responses

The time series of the broadband and stimulus-locked responses to bar stimuli were constructed by short-time Fourier analysis, as previously (Winawer et al., 2013), with one difference. The stimulus-locked time series was defined by the amplitude at 30Hz, twice the frequency of stimulus contrast reversals, rather than at the frequency of stimulus contrast reversals, as there was a higher signal to noise ratio at this harmonic. Details are included in the Supplemental Methods.

Electrical Brain Stimulation

Electrical biphasic, rectangular pulses were delivered at different frequency, pulse width, amplitude, and durations (Table S2). These pulses were current-regulated and charge balanced (i.e., no charge accumulation with toxic effect on the tissue). For each site, one electrode was in V1 and the other was in a non-visually responsive region, remote from V1. Occasional sham trials were intermixed with stimulation trials. The subjects were not informed which trials were sham and which contained stimulation. EBS trials took place 1–2 days after ECoG visual mapping experiments (see Table S2 for more details).

Phosphene recordings

During the EBS sessions, subjects viewed the same laptop used for the ECoG visual mapping experiments, viewed from the same distance. Subjects were instructed to fixate the center of a polar grid prior to EBS (Figure 3b), and to draw the outline of their visual percept on the screen using the laptop touchpad immediately following stimulation. The polar grid provided a spatial reference so that subjects could accurately encode and reproduce the location of the phosphene. Offline, the phosphene outlines were loaded into Matlab and digitized (Figure S3). Phosphene-pRF overlap was summarized by the Dice Coefficient (Eq S2) and bootstrapped for statistics (Eq S3).

Subjective ratings

Subjective ratings of phosphene intensity were obtained immediately after drawing the phosphene outline for sites 2, 3, and 5. For site 3 and 5 (S3), the subject was instructed to indicate on a scale from 0–10 how much motion, color, and brightness was in each phosphene. It appeared that the subject did not use the ratings independently, as the three ratings were almost always the same for a given phosphene. Hence we collapsed the three ratings per trial into one (using the median if the three were not identical). For S2, whose experiment took place later, we asked for only a single rating of 0–10 to indicate the intensity of the percept.

Computation of phosphene cortical area

Phosphenes were projected to the surface of V1 based on the subject's retinotopic map in order to infer the area of activated cortex resulting from EBS. The projection was defined as the set of voxels in V1 whose retinotopic coordinates (x, y) were within the polygon defined by the digitized phosphene. These voxels formed a region of interest, and the surface area of this region of interest was computed on the 3D cortical manifold using methods described previously (Dougherty et al., 2003). The Matlab function used for this computation is 'roiSurfaceArea', part of the freely available in-house vistasoft software (https://github.com/vistalab/vistasoft). The cortical surface area was also estimated using a standard formula that did not depend on each subject's maps (see Supplemental Methods).

Data Availability

The software and data used for analyses is available via the Open Science Framework (https://osf.io/pz42u/, DOI 10.17605/OSF.IO/PZ42U)

Supplementary Material

Refer to Web version on PubMed Central for supplementary material.

Acknowledgments

We thank Noah Benson for expert assistance in deriving retinotopic templates for visual cortex. The research was supported by US National Eye Institute (EY022116) to J.W., and US National Institute of Neurological Disorders and Stroke (R01NS078396), US National Institute of Mental Health (1R01MH109954-01) and US National Science Foundation (BCS1358907) to J.P.

References

Adrian ED, Matthews BHC. The Berger rhythm: Potential changes from the occipital lobes in man. Brain. 1934; 57:355–385.

Bartholow R. Art. I.-Experimental Investigations into the Functions of the Human Brain. The American Journal of the Medical Sciences. 1874; 66:305–313.

Benson NC, Butt OH, Brainard DH, Aguirre GK. Correction of distortion in flattened representations of the cortical surface allows prediction of V1-V3 functional organization from anatomy. PLoS Comput Biol. 2014; 10:e1003538. [PubMed: 24676149]

Borchers S, Himmelbach M, Logothetis N, Karnath HO. Direct electrical stimulation of human cortex - the gold standard for mapping brain functions? Nature reviews Neuroscience. 2012; 13:63–70.

Brindley GS, Lewin WS. The sensations produced by electrical stimulation of the visual cortex. J Physiol. 1968; 196:479–493. [PubMed: 4871047]

Buzsaki G, Anastassiou CA, Koch C. The origin of extracellular fields and currents--EEG, ECoG, LFP and spikes. Nature reviews Neuroscience. 2012; 13:407–420. [PubMed: 22595786]

Canolty RT, Edwards E, Dalal SS, Soltani M, Nagarajan SS, Kirsch HE, Berger MS, Barbaro NM, Knight RT. High gamma power is phase-locked to theta oscillations in human neocortex. Science. 2006; 313:1626–1628. [PubMed: 16973878]

Cohen MR, Newsome WT. What electrical microstimulation has revealed about the neural basis of cognition. Current opinion in neurobiology. 2004; 14:169–177. [PubMed: 15082321]

Crick F, Koch C. Are we aware of neural activity in primary visual cortex? Nature. 1995; 375:121–123. [PubMed: 7753166]

Crone NE, Miglioretti DL, Gordon B, Lesser RP. Functional mapping of human sensorimotor cortex with electrocorticographic spectral analysis. II. Event-related synchronization in the gamma band. Brain. 1998; 121(Pt 12):2301–2315. [PubMed: 9874481]

Dobelle WH, Mladejovsky MG. Phosphenes produced by electrical stimulation of human occipital cortex, and their application to the development of a prosthesis for the blind. J Physiol. 1974; 243:553–576. [PubMed: 4449074]

Dougherty RF, Koch VM, Brewer AA, Fischer B, Modersitzki J, Wandell BA. Visual field representations and locations of visual areas V1/2/3 in human visual cortex. J Vis. 2003; 3:586–598. [PubMed: 14640882]

Dumoulin SO, Wandell BA. Population receptive field estimates in human visual cortex. Neuroimage. 2008; 39:647–660. [PubMed: 17977024]

Foerster O. Beitriige zur Pathophysiologie der Sehbahn und der Sehsphare. Journal of Psychology and Neurology. 1929; 39:463–485.

Hermes D, Miller KJ, Noordmans HJ, Vansteensel MJ, Ramsey NF. Automated electrocorticographic electrode localization on individually rendered brain surfaces. Journal of neuroscience methods. 2010; 185:293–298. [PubMed: 19836416]

Hinds OP, Rajendran N, Polimeni JR, Augustinack JC, Wiggins G, Wald LL, Diana Rosas H, Potthast A, Schwartz EL, Fischl B. Accurate prediction of V1 location from cortical folds in a surface coordinate system. Neuroimage. 2008; 39:1585–1599. [PubMed: 18055222]

Histed MH, Bonin V, Reid RC. Direct activation of sparse, distributed populations of cortical neurons by electrical microstimulation. Neuron. 2009; 63:508–522. [PubMed: 19709632]

Kay KN, Winawer J, Mezer A, Wandell BA. Compressive spatial summation in human visual cortex. Journal of neurophysiology. 2013; 110:481–494. [PubMed: 23615546]

Kitano M, Niiyama K, Kasamatsu T, Sutter EE, Norcia AM. Retinotopic and nonretinotopic field potentials in cat visual cortex. Vis Neurosci. 1994; 11:953–977. [PubMed: 7947408]

Linden H, Tetzlaff T, Potjans TC, Pettersen KH, Grun S, Diesmann M, Einevoll GT. Modeling the spatial reach of the LFP. Neuron. 2011; 72:859–872. [PubMed: 22153380]

Liu J, Newsome WT. Local field potential in cortical area MT: stimulus tuning and behavioral correlations. J Neurosci. 2006; 26:7779–7790. [PubMed: 16870724]

Miller KJ, Honey CJ, Hermes D, Rao RP, denNijs M, Ojemann JG. Broadband changes in the cortical surface potential track activation of functionally diverse neuronal populations. Neuroimage. 2014; 85(Pt 2):711–720. [PubMed: 24018305]

Miller KJ, Sorensen LB, Ojemann JG, den Nijs M. Power-law scaling in the brain surface electric potential. PLoS Comput Biol. 2009; 5:e1000609. [PubMed: 20019800]

Milstein J, Mormann F, Fried I, Koch C. Neuronal shot noise and Brownian 1/f2 behavior in the local field potential. PloS one. 2009; 4:e4338. [PubMed: 19190760]

Mitzdorf U. Properties of the evoked potential generators: current source-density analysis of visually evoked potentials in the cat cortex. Int J Neurosci. 1987; 33:33–59. [PubMed: 3610492]

Norcia AM, Appelbaum LG, Ales JM, Cottereau BR, Rossion B. The steady-state visual evoked potential in vision research: A review. J Vis. 2015; 15:4.

Ojemann G, Ojemann J, Lettich E, Berger M. Cortical language localization in left, dominant hemisphere. An electrical stimulation mapping investigation in 117 patients. J Neurosurg. 1989; 71:316–326. [PubMed: 2769383]

Palmer CR, Chen Y, Seidemann E. Uniform spatial spread of population activity in primate parafoveal V1. Journal of neurophysiology. 2012; 107:1857–1867. [PubMed: 22170967]

Penfield W, Perot P. The Brain's Record of Auditory and Visual Experience. A Final Summary and Discussion. Brain. 1963; 86:595–696. [PubMed: 14090522]

Salzman CD, Britten KH, Newsome WT. Cortical Microstimulation Influences Perceptual Judgments of Motion Direction. Nature. 1990; 346:174–177. [PubMed: 2366872]

Stevens SS. On the psychophysical law. Psychol Rev. 1957; 64:153–181. [PubMed: 13441853]

Tehovnik EJ, Slocum WM. Phosphene induction by microstimulation of macaque V1. Brain Res Rev. 2007; 53:337–343. [PubMed: 17173976]

Wandell, BA. Foundations of vision. Sunderland, Mass: Sinauer Associates; 1995.

Winawer J, Kay KN, Foster BL, Rauschecker AM, Parvizi J, Wandell BA. Asynchronous broadband signals are the principal source of the BOLD response in human visual cortex. Curr Biol. 2013; 23:1145–1153. [PubMed: 23770184]

Yoshor D, Bosking WH, Ghose GM, Maunsell JH. Receptive fields in human visual cortex mapped with surface electrodes. Cerebral cortex. 2007; 17:2293–2302. [PubMed: 17172632]

Highlights

- Electrical brain stimulation in patients with electrodes in V1 elicited phosphenes
- Phosphenes matched the electrode receptive field measured with broadband potentials
- Phosphene size increased systematically with eccentricity and amount of charge
- Cortical area activated increased with the amount of charge but not eccentricity

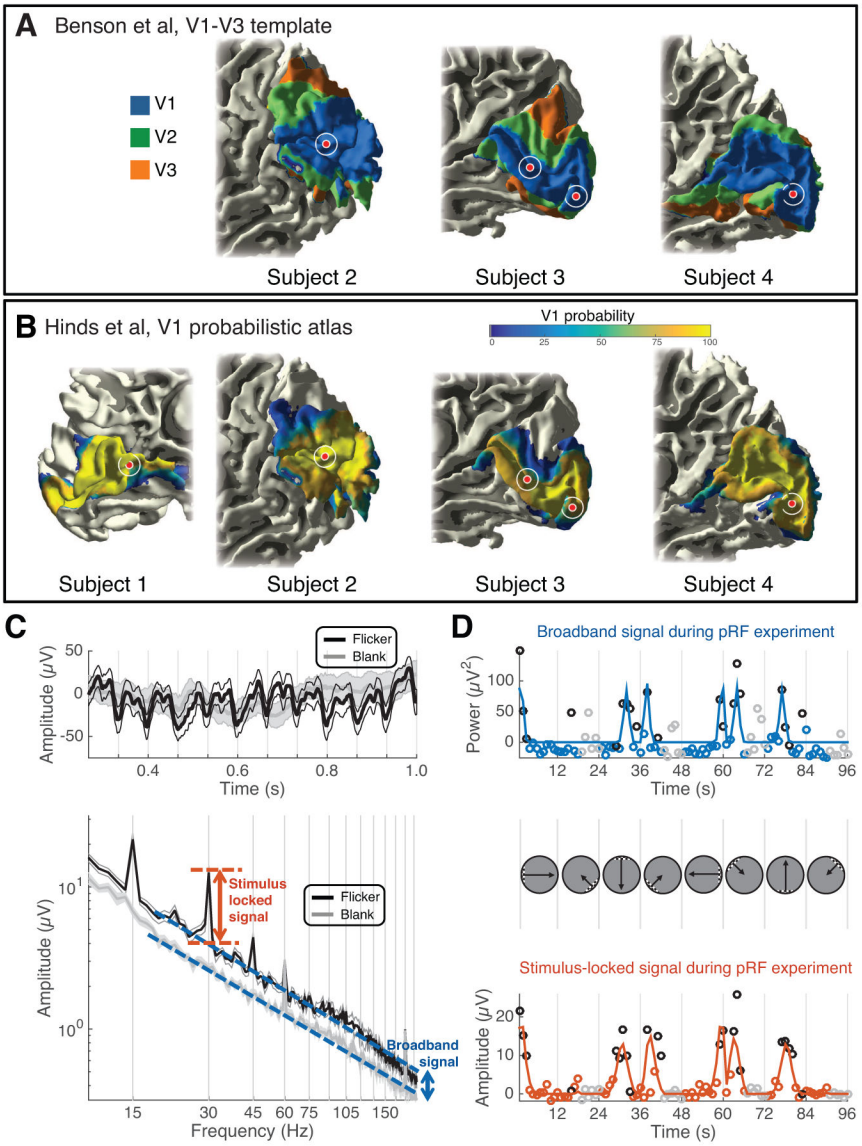

Figure 1. Electrophysiological signals in V1 electrodes

(A–B) A template of V1-V3 (Benson et al., 2014) and a probabilistic atlas of V1 (Hinds et al., 2008) were applied to each subject's T1-weighted anatomical MRI. The electrodes used for EBS are shown as red circles. The white circle indicates positional uncertainty of 5 mm in radius. All electrodes are within the Benson template V1 (the template failed on subject 1 due to poor alignment with the standard anatomical image in FreeSurfer) and high probability areas of the Hinds V1. (C) Mean time series (top) and power spectra (bottom) from several 1-s epochs during visual mapping experiments from an example V1 electrode (site 2). The traces show data averaged across 24 epochs when the bar stimulus was near the site's pRF (black), or when the stimulus was blank (gray). The shaded region indicates ±1 SEM across 24 epochs. The arrows depict the stimulus locked (orange) and broadband signals (blue). (D) The 96-s experiment was summarized with two time series, broadband (upper) and stimulus-locked (lower). The trajectory of the bar apertures is shown between

the upper and lower plots. Blue and orange lines are pRF model fits to the data, and circles are the data (either broadband or stimulus locked measurement from each epoch). Black and gray circles indicate the 24 epochs summarized in panel C (flicker and blank, respectively). See Figure S1, Table S1.

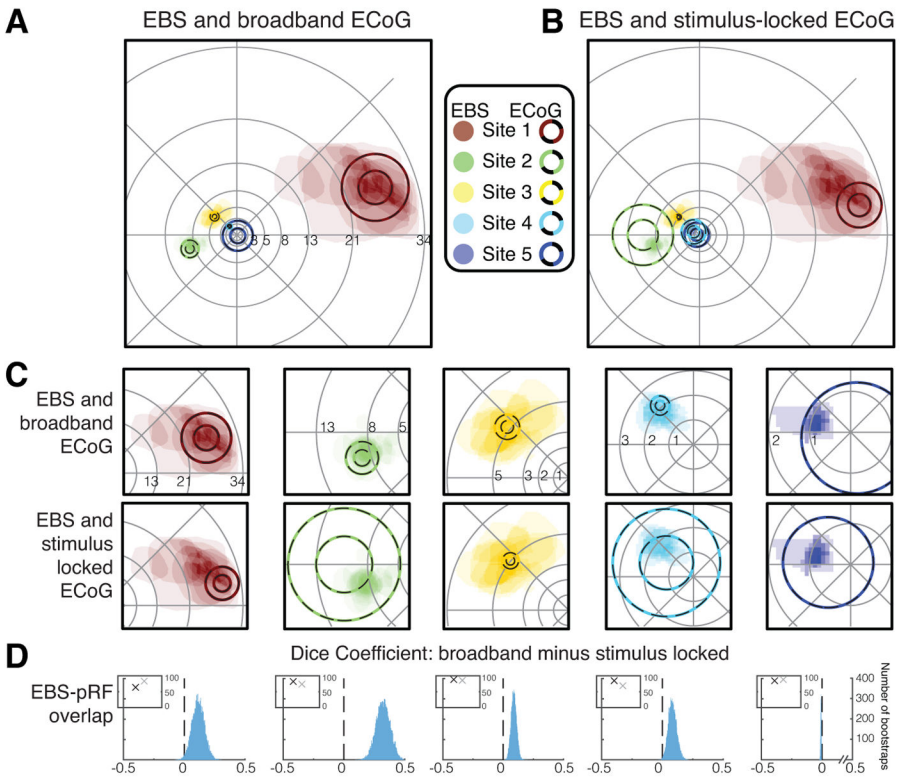

Figure 2. Comparison of spatial selectivity between EBS and ECoG

(A) A comparison of pRFs derived from broadband ECoG data (circles, 1- and 2-SD lines) and phosphenes drawn by subjects (shaded regions). The number of phosphenes drawn for the 5 sites was 18, 21, 16, 18, and 9 (Sites 1–5). (B) Same as A except that pRFs are derived from the stimulus-locked ECoG data. (C) Zoom of the data from A (upper plots) and B (lower plots). (D) Each histogram shows the difference in overlap (Dice coefficient) between the phosphenes and broadband pRF versus the phosphenes and stimulus-locked pRFs. A positive number on the x-axis means greater overlap between the phosphene and broadband pRF than between the phosphene and stimulus-locked pRF. Histograms were derived by bootstrapping over stimulation trials. For sites 1–4, the overlap with the broadband pRF is greater than with the stimulus-locked pRF (histograms to the right of 0). For site 5, the pRF is very foveal and not accurately estimated by the ECoG data, hence the overlap coefficient is low for both types of pRFs. Insets show variance explained by the pRF models (black=broadband; gray=stimulus-locked). The variance explained is similar for the two types of pRF models. See Figures S2, S3, Tables S2, S3.

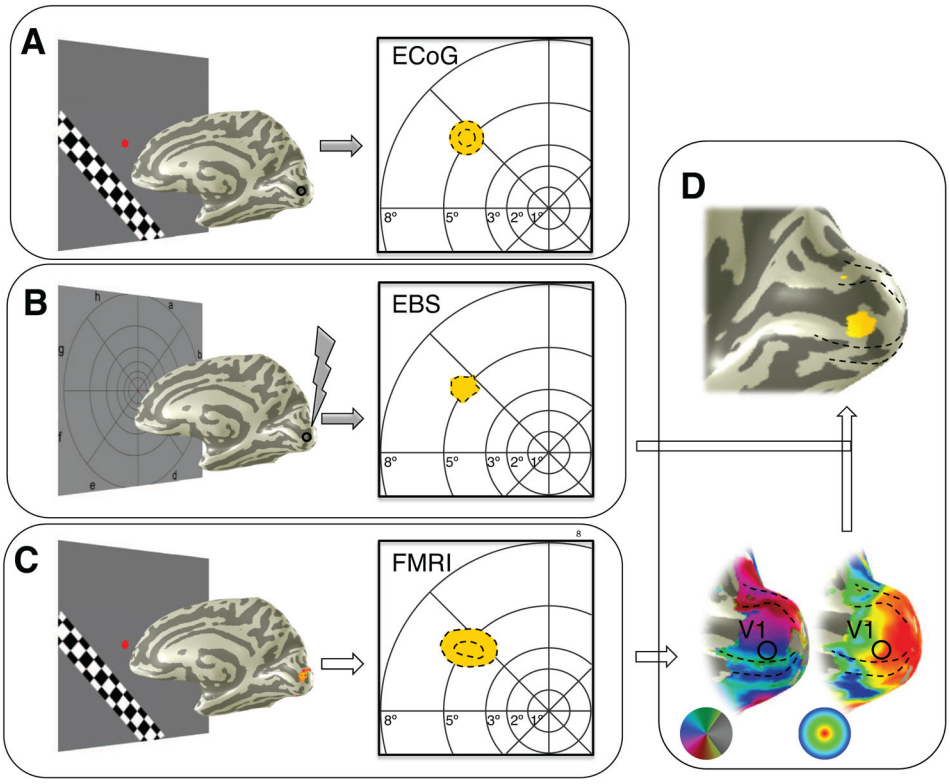

Figure 3. Spatial selectivity in human visual cortex across 3 measurement modalities

(A) A pRF (yellow circle) was computed for the broadband ECoG signal in response to visual stimulation (site 3). Dotted lines show the 1-, and 2-std lines of the pRF for the electrode indicated on the cortical mesh, as in Figure 2A. (B) The subject drew the outline of a phosphene during an EBS trial (black dotted line). (C) The combined fMRI pRFs for voxels near the electrode shown in A and B. Dotted lines as in A. (D) The phosphene in B was projected onto the cortical surface using the retinotopic map of visual cortex, derived from fMRI.

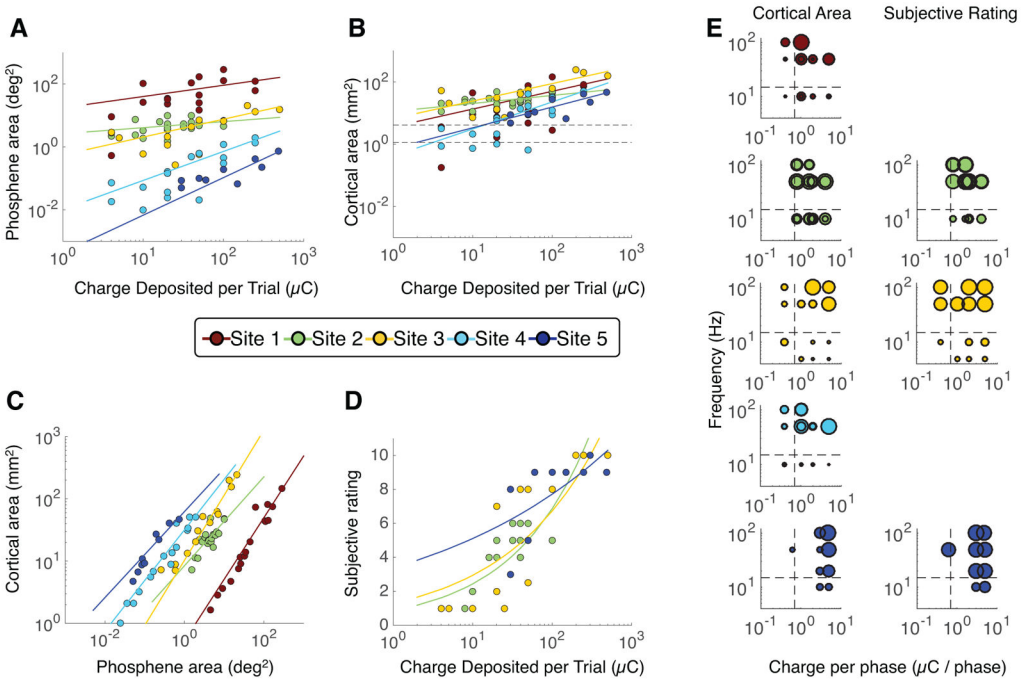

Figure 4. Relationship between perception and EBS parameters

For all panels, each dot indicates one EBS trial and each color indicates one cortical site. Sites 1 to 5 are numbered by decreasing eccentricity of the site's pRF: site 1 is most peripheral and site 5 is most foveal. For panels A–D, colored lines are the best fitting power functions of the form $y=b*x^m$, fit separately for each site. For parameters and details of fits, see Table S3. Greater charge deposited per EBS trial resulted in (A) larger phosphenes, (B) a larger area of activated cortex (inferred by projecting the phosphenes onto each subjects' V1 surface), and (D) a higher subjective intensity rating. The fitted power law exponents are less than 1, indicating that the stimulation effect saturates at high charge. In panel B, dashed lines indicate the electrode's exposed surface area (upper line for sites 1, 3, 4, and 5; lower line for site 2; see Table S2). Panel C shows the relationship between phosphene area in the visual field (x-axis) and cortical area (phosphene projected to V1). (E) The bubble plots separate the charge delivered per trial into charge per phase (x-axis) and frequency (y-axis). Each bubble indicates one trial, and bubble size reflects either cortical area (left column) or subjective rating (right column). The largest bubble in each plot is scaled to the maximum measurement for that plot (panel B for cortical area and panel D for subjective rating). Dashed lines indicate the stimulation levels which approximately divide the cortical area into large and small values. For a linear model fit to the data in panel E, see Figure S4 and Table S4.